Cell Reports
Physical Science

CellPress
OPEN ACCESS

Article

Efficient single-molecular white-light emission for iridium-based photoluminescent and electroluminescent white OLEDs

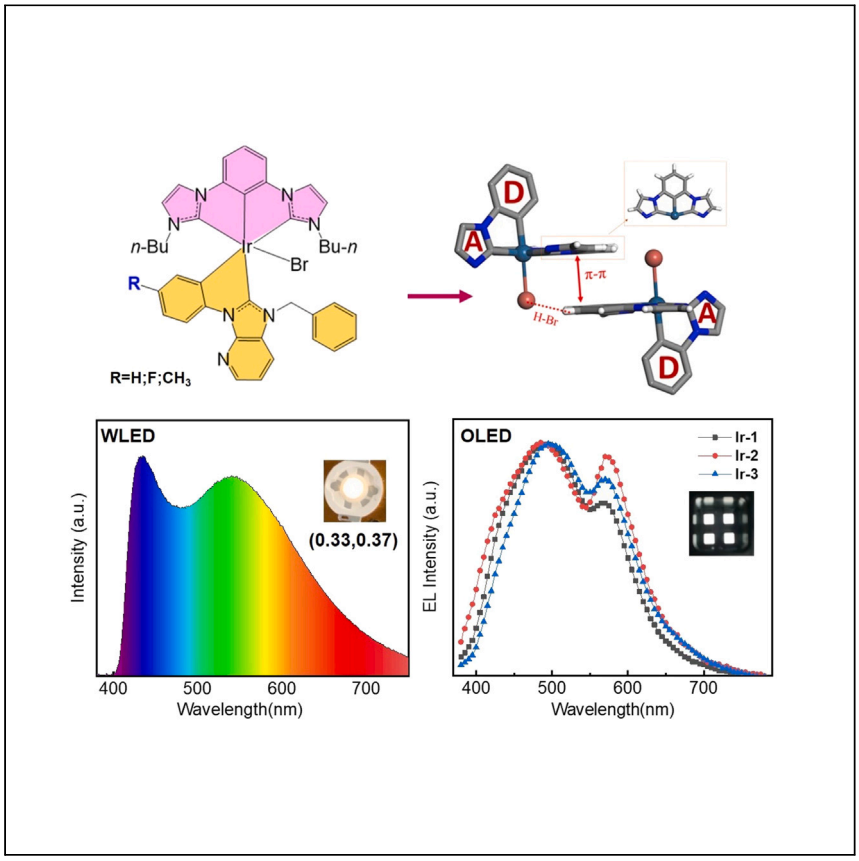

Zhang et al. report a series of single-component white-light emitters based on iridium(III) complexes that can be used as color converters in solid-state white light-emitting diodes with nearly standard white light. The vacuum-deposited OLED device based on them achieves white emission by only a single-component emitting layer.

Meng Zhang, Wansi Li, Si-Wei Zhang, ..., Chao He, Guodan Wei, Feiyu Kang

kobetang2021@sz.tsinghua.edu.cn (M.-C.T.)
david_yang@purimat.com (C.Y.)
weiguodan@sz.tsinghua.edu.cn (G.W.)

Highlights

Single-component white-light emitters are obtained based on iridium complexes

High-energy blue and low-energy yellow emission form the white light

The white LEDs show a high color rendering index of 86.2

The white OLED device exhibits CIE coordinates of (0.31, 0.33)

Zhang et al., Cell Reports Physical Science 4, 101684
December 20, 2023
https://doi.org/10.1016/j.xcrp.2023.101684

Cell Reports
Physical Science

CellPress
OPEN ACCESS

Article

Efficient single-molecular white-light emission for iridium-based photoluminescent and electroluminescent white OLEDs

Meng Zhang,[1,2,7] Wansi Li,[1,2,7] Si-Wei Zhang,[1,2,7] Maggie Ng,[2] Chengcheng Wu,[1,2] Man-Chung Tang,[2,*] Yuan Wu,[3] Chen Yang,[3,*] Hong Meng,[4] Jianwei Zhao,[5] Chao He,[6] Guodan Wei,[1,2,8,*] and Feiyu Kang[2]

SUMMARY

The white organic light-emitting diode has become as a new class of emerging solid-state lighting sources due to its advantage of warm, pure white light emission, flexible lighting, and environmentally friendly indoor lighting. Here, we report three rationally designed cyclometalated [3 + 2+1] iridium(III) complexes that emit white emission simultaneously from phosphorescent blue and yellow in the solid-state thin film. The blue GaN-based solid-state white light-emitting diodes with iridium(III) complexes as a color converter show a color rendering index of 84.4 and International Commission on Illumination (CIE) coordinates of (0.30, 0.33). In addition, the vacuum-deposited organic light-emitting diode device exhibits a low turn-on voltage of 3.0 V and a maximum luminance (L_{max}) of 335 cd m^{-2} with CIE coordinate of (0.31, 0.33), reaching standard naturally warm white light.

INTRODUCTION

White organic light-emitting diodes (WOLEDs) have gradually become attractive candidates for energy-saving and environmentally friendly solid-state lighting sources attributed to their high color rendering index (CRI), mechanical flexibility, high-quality white emission, and low-cost fabrication.[1–3] It has been recently reported that the integration of green- to red-emitting phosphors into blue light-emitting chips could demonstrate a comparable power efficiency to the state-of-the-art white light-emitting diodes (WLEDs).[4] In this case, WOLED devices could be fabricated by vertically stacking multi-emissive layers (or multiple components) for the mixing of primary colors (red, green, and blue [RGB]) or two complementary colors (blue with yellow or orange).[5,6] However, these WOLED devices require complicated multi-layer thin film deposition processes and balanced electron and hole injection, leading to a great challenge including the phase separation of emitters and voltage-dependent emission color in the emissive layer.[7–10]

To realize white-light emission based on a single organic molecule,[4,11] emitters with a broad emission spectrum covering the whole visible region and dual emission are commonly used. For fluorescent emitters, the blue emissions come from the π–π^* intraligand transition, and the yellow/orange emission comes from the intramolecular charge transfer,[12] intermolecular interactions (dimer or excimer),[13] partially excited energy transfer,[14] and excited-state proton transfer.[15] However, these require strict molecular orientation such as single-crystal characteristics and usually generate fluorescence with relatively low internal quantum efficiency.[4] Lately, taking

[1]Tsinghua-Berkeley Shenzhen Institute (TBSI), Tsinghua University, Shenzhen 518055, China

[2]Institute of Materials Research, Tsinghua Shenzhen International Graduate School, Tsinghua University, Shenzhen 518055, China

[3]PURI Materials, Shenzhen 518133, China

[4]School of Advanced Materials, Peking University, Shenzhen Graduate School, Peking University, Shenzhen 518055, China

[5]Shenzhen HUASUAN Technology Co., Ltd, Shenzhen 518055, China

[6]Department of Engineering Science, University of Oxford, Parks Road, Oxford OX1 3PJ, UK

[7]These authors contributed equally

[8]Lead contact

*Correspondence: kobetang2021@sz.tsinghua.edu.cn (M.-C.T.), david_yang@purimat.com (C.Y.), weiguodan@sz.tsinghua.edu.cn (G.W.)

https://doi.org/10.1016/j.xcrp.2023.101684

advantage of the metal-metal interaction that facilitates the intermolecular interaction of square-planar d^8 platinum(II)[16,17] and linear d^{10} gold(I), they have been reported as single-component emitters and successfully fabricated as WOLEDs with promising performance.[18,19] Meanwhile, the report of the octahedral d^6 iridium(III) complexes as single-component white emitters has been rarely reported, even though iridium(III) complexes show short phosphorescence lifetime, excellent thermal and device stabilities and are commonly used as dopants for OLEDs.[20,21] Therefore, the development of single-component white-light emitters based on iridium(III) complexes by manipulating their emissive states through ligand engineering is anticipated.[22–29]

For instance, Zhang et al. reported a series of dual phosphorescence iridium(III) complexes. Photophysical measurement and time-dependent density functional theory (TD-DFT) calculation revealed that the dual emission was attributed to the rapid conversion of IL (intraligand) charge transfer (CT) to ligand-ligand CT (LLCT) excited states.[24] Structural manipulation of the iridium(III) complexes exhibits naked-eye distinguishable color changes in the aqueous buffer solution under the different atmospheres of N_2, air, and O_2, respectively.[24] Sarvendra Kumar et al. reported heteroleptic cyclometalated iridium(III) complexes with quinoline-type ligands whose dual emission originates from two independent emissions states.[23] However, these dual-phosphorescent emissions iridium(III) complexes occur in the solution state but not in the film state, which limits their application for WOLED.

With the experience in the development of [3 + 2+1] coordinated phosphorescent iridium(III) complexes,[2,30–32] we design three iridium(III) bromine complexes bearing bidentate (*N*-phenyl, *N*-benzyl-pyridoimidazol-2-yl) (C^C) ligands for bright white-light emission in solid-state state (powder or thin film) at room temperature. For all iridium(III) complexes, the white light comes from dual-phosphorescent emission at the high-energy blue and low-energy yellow regions. Upon introducing electron-donating methyl, or electron-withdrawing fluorine group onto the 4-position of the phenyl of C^C ligand, the phosphorescent quantum efficiency of these iridium(III) complexes in the solid state increase from 3.1% to 14.1%, which is due to the increased $\pi-\pi^*$ interaction between the tridentate ligands of two adjacent molecules of fluorinated iridium complexes (**Ir-2**). In addition, the molecular orientation and stacking order affect the emission energies, which is supported by experimental and the DFT and TD-DFT calculations. Finally, the performances of the WLEDs based on **Ir-2** and the OLED with **Ir-2** as an active layer are measured and evaluated.

RESULTS AND DISCUSSION

Molecular synthesis and characterization

In this work, the ligands around iridium are redistributed to achieve a robust intermolecular interaction, as shown in Figure 1C. Three coordination bonds are occupied with forming a rigid planar, desired moiety for intermolecular interaction. Then a bidentate ligand armed with a strong donor-accept (D-A) chromophore is grafted on the remaining two iridium coordinations. In addition, a monodentate ligand with a small steric hindrance is adopted to narrow intermolecular distance. This molecular structure design strategy enables monomer luminescence and dimer luminescence simultaneously.

Molecular structures of iridium(III) complexes are shown in Figure 1A, and the synthetic route is shown in Scheme S1. In brief, the tridentate bis-N-heterocyclic-carbene (NHC) pincer ligand **pbib** and bidentate ligands (**pmpBz**, **pmpFBz**, and

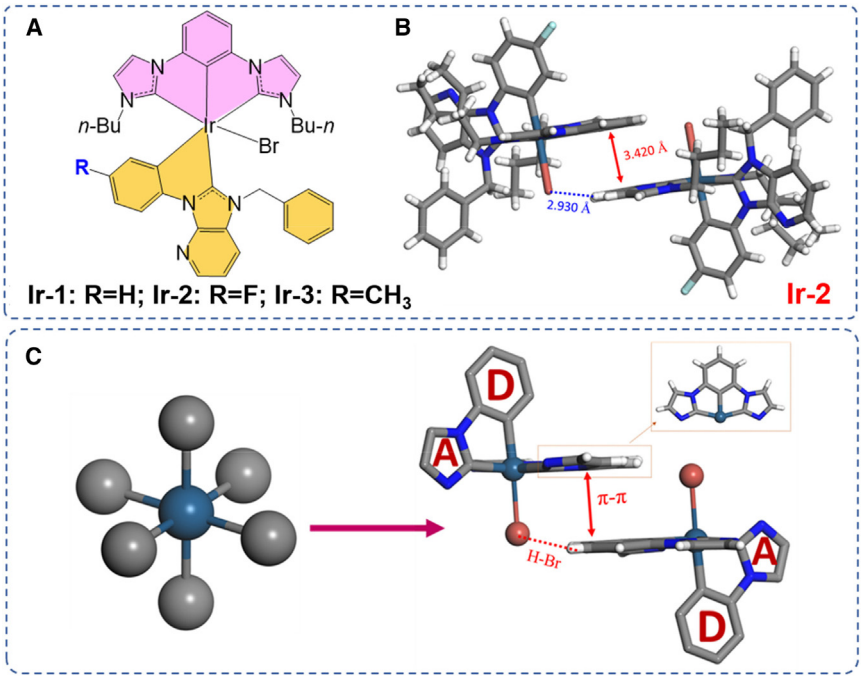

Figure 1. Molecular and crystal structures

(A) Molecular structures of **Ir-1-3** studied here.

(B) Single-crystal structure of **Ir−2**.

(C) Design strategy for iridium(III) complexes with dual emission.

pmpMeBz) were synthesized according to the previously reported literature.[33,34] Subsequently, the **pbib** and bidentate ligands reacted with the iridium(III) precursor complex $[Ir(COD)Cl]_2$ and obtained the solid-state single-component white-light iridium(III) complexes **Ir-1**, **Ir-2**, and **Ir-3**, respectively. The iridium(III) complexes were confirmed by ^{1}H, ^{19}F, and ^{13}C nuclear magnetic resonance spectroscopies (Figures S1–S18) and high-resolution electrospray ionization mass spectroscopy (Figures S19–S21).

The single-crystal structure of **Ir-2** confirms the validity of the design strategy (Figures 1B and S23). The tridentate NHC pincer ligand **pbib** is a rigid planar structure, and the bond lengths of Ir−C(1), Ir−C(9), and Ir−C(10) are 2.057, 2.013, and 2.068 Å, which are consistent with the corresponding data of [3 + 2+1] iridium(III) complexes we reported before. The emission color of these [3 + 2+1] iridium(III) complexes can be fine-tuned by modifying the structure of the bidentate ligand.[35] In addition, the (D-A) fragment and **pbib** plane are almost perpendicular, reducing the distortion of the molecular structure. The main single-crystal structure parameters are listed in Tables S1–S3. Furthermore, as shown in Figures 1B and S24, the monodentate halogen ligand (distance of Br … H is 2.930 Å) and other intermolecular interactions narrow the distance between the two molecules. The distance between the two **pbib** planes is 3.420 Å, which is sufficient for energy transfer or interaction. The single-crystal of **Ir-2** shows a white light with dual emissions, as shown in Figure S25.

In order to investigate the photophysical properties of these complexes, a series of photophysical measurements were performed. Firstly, we characterized the absorption spectra of **Ir-1-3** in degassed dilute dichloromethane (DCM) solutions

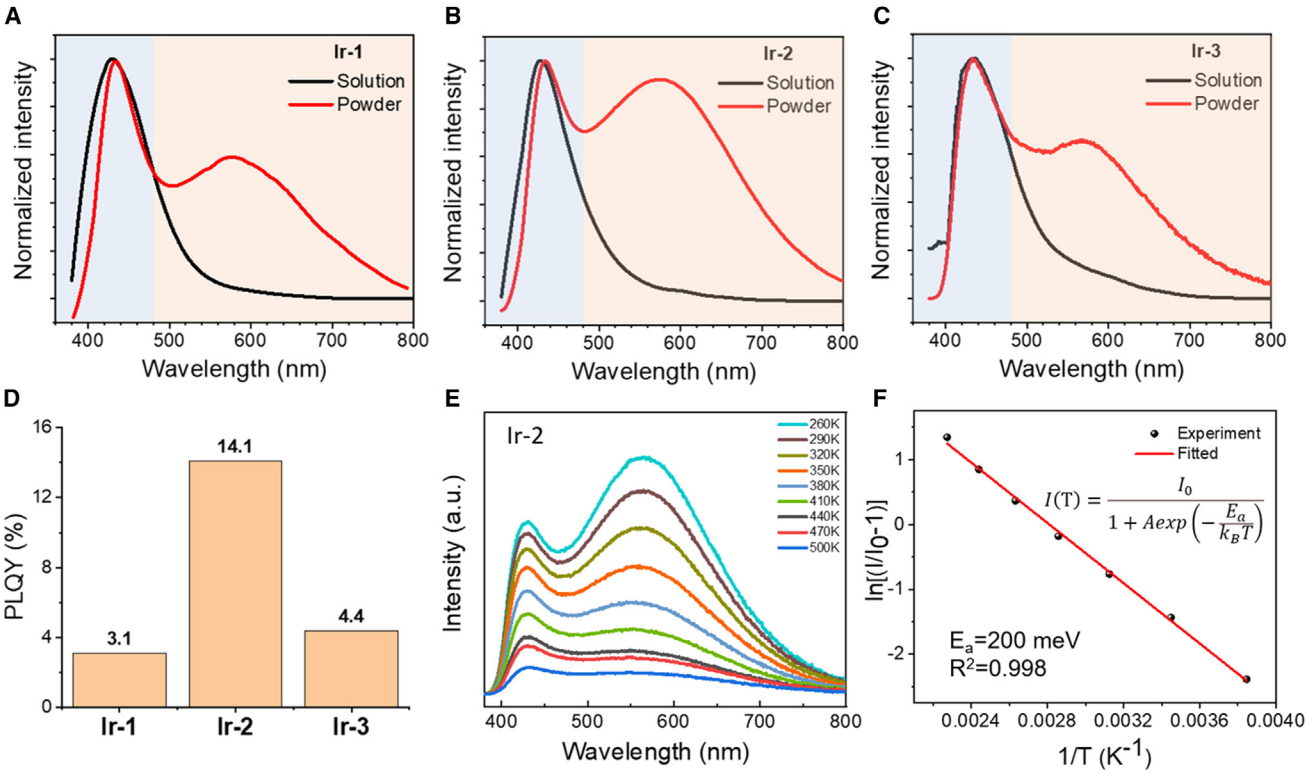

Figure 2. The emission prosperities of Ir-1-3

(A–C) The PL spectra in solution (c = 2 × 10^{-5} M in DCM) and powder state of (A) **Ir-1**, (B) **Ir-2**, and (C) **Ir-3**.

(D) The PLQY of **Ir-1-3** complexes in powder state.

(E) **Ir-2** temperature-dependent PL spectra taken from 260 to 500 K.

(F) The ln[(I/I_0−1] as a function of 1/T and the calculated activation energy (E_a) of **Ir-2** in solid.

($c = 2 \times 10^{-5}$ M) to investigate the photophysical properties of the unimolecular. As shown in Figure S26, **Ir-1-3** shows a similar absorption spectrum (**Ir-2** [312 nm] > **Ir-1** [313 nm] > **Ir-3** [314 nm]), which indicated that the introduction of the -F then -H and -CH_3 onto the bidentate ligand does not alter the absorption energies, and it is possible such an effect has imposed a similar effect on the HOMO and LUMO and thus cancels out. While the strong absorption around 310 nm ($\epsilon \approx 10^4$ $M^{-1}cm^{-1}$) is assigned the spin-allowed singlet $^1(\pi \rightarrow \pi^*)$ and metal to ligand charge transfer (^{1}MLCT) transitions. The weak absorption bands ($\epsilon \approx 10^3$ $M^{-1}cm^{-1}$) lying in the visible light region at 350–400 nm are related to the spin-orbit coupling enhanced triple $^3(\pi \rightarrow \pi^*)$ transitions and metal to ligand charge transfer (^{3}MLCT) transitions.[36]

The emission spectra and their photophysical properties of **Ir-1-3** are shown in Figures 2A–2C and Table 1. **Ir-1-3** shows faint blue emission in degassed diluted solution with a peak at 429 nm, 427 nm, and 433 nm, respectively. Similar to their absorption spectra, the emission energies are only slightly perturbed by the introduction of the -H, -CH_3, and -F groups. Unlike the white emission of these complexes in the solution state that is not detectable, the powder form of **Ir-1-3** showed white emission at ambient including dual peaks similar to the single crystal. The difference between emission spectra in solution and solid is illustrated in Figure S27. The **Ir-1-3** complexes were doped in a thin polymethylmethacrylate (PMMA) polymer film (at x wt %, x = 20, 40, 60, 80) at ambient temperature, the emission spectra of complexes in different molecular states were obtained. White-light emission in solid state is desired to realize photoluminescence/electroluminescence applications. The sharp

Table 1. The emission properties of Ir-1-3 in dilute and solid powder

	In dilute solution[a]				In powder			
Complex	Absorption λ_{max}(nm)	Emission λ_{max}(nm)	τ (μs)	PLQY[b]	Emission λ_{max}(nm)	τ[c] (μs)	CIE	PLQY (%)
Ir-1	313	429	0.65	–	432, 577	0.98, 1.05	(0.29, 0.28)	3.1
Ir-2	312	427	0.72	–	431, 578	1.12, 1.36	(0.30, 0.32)	14.1
Ir-3	314	433	0.89	–	433, 573	1.21, 1.38	(0.28, 0.27)	4.4

[a]Data were measured in degassed DCM at 2 x 10^{-5} M.
[b]"–" means the data are too weak to measure.
[c]The lifetime of high-energy peak and low-energy peak, respectively.

peaks in the X-ray diffraction pattern suggest the crystallization behavior in the powder (Figure S28). The high energy peak position at the blue region is similar to the emission's character in dilute solutions. In addition, the **Ir-1-3** in solid state shows a relatively higher PLQY (photoluminescence quantum yield) than the dilute solution, benefiting the practical application. White emission with International Commission on Illumination (CIE) coordinates of (0.30, 0.32) is achieved from the powder of **Ir-2**, which was quite close to the pure white color of CIE coordinate (0.33, 0.33). The possible reason for higher PLQY and better CIE of **Ir-2** is the existence of -F, which forms two H ··· F (2.542 å) bonds (Figure S24) and enhances the intermolecular forces and molecular rigid. It is obvious that the low-energy peak intensity of **Ir-2** is higher than the high-energy peak intensity, which is the opposite trend of **Ir-1** and **Ir-3**. The time-resolved photoluminescence spectrum in Figure S29 certified that both peaks are phosphorescent. The excitation spectra of high-energy and low-energy peaks verifies that these dual-phosphorescent emissions originate from two different excited states (Figure S30).

Additionally, the emission spectra of complex **Ir-2** in solid under constant temperature control from 260 to 500 K were also tested. As observed in Figure 2E, the intensity of the luminescence spectra decreased with temperature increased due to thermal quenching. It is worth noting that at low temperatures, the intensity of the low-energy peak (ca. 570 nm) is much higher than that of the high-energy peak (ca. 430 nm). At room temperature, their intensity is comparable, which is consistent with the emission spectrum in the powder state. The activation energy (E_a) can be obtained by the following equation:

$$I(T) = \frac{I_0}{1+Aexp\left(-\frac{E_a}{k_B T}\right)} \quad \text{(Equation 1)}$$

where I(T) is the integrated photoluminescent intensity at temperature T and I_0 is that at initial temperature. A is a constant, and k_B is Boltzmann's constant. According to the temperature-dependent PL spectra of **Ir-2** in solid, we got the calculated activation energy (E_a) of 200 meV (Figure 2F), indicating high thermal stability and a very promising candidate for white light illumination.

The electrochemical properties of the complex **Ir-1-3** were also investigated by cyclic voltammetry in degassed DCM solutions (0.1 M $^{n}Bu_4NPF_6$). Figure S31 shows their cyclic voltammograms, while electrochemical data are displayed in Table 2. Similar to the previously reported literature, no significant reduction peaks were observed. While complex **Ir-1-3** shows a quasi-reversible couple or irreversible first oxidation wave at ca. +0.95 V vs. saturated calomel electrode (SCE). This may be due to the oxidation of the NHC bidentate carbene ligands (C^C).[37] All the assignments are in line with the TD-DFT calculations.

Table 2. Electrochemical data of the Ir-1-3 complexes

Complex	Oxidation[a] $E_{1/2}$ [V] vs. SCE[b] (ΔE_p [mV])[c] [E_{pa} [V] vs. SCE][d]	E_{HOMO} [eV][e]	E_{LUMO} [eV][f]
Ir-1	+0.95 (95)	−5.29	−2.17
Ir-2	+0.96	−5.30	−2.11
Ir-3	+0.91	−5.21	−2.13

[a]In DCM solution with 0.1 M.$^{n}Bu_4NPF_6$ as supporting electrolyte at 298 K working electrode, glassy carbon; scan rate = 100 mV^{-1}.
[b]$E_{1/2} = (E_{pa} + E_{pc})/2$; E_{pa} and E_{pc} are the peak anodic and peak cathodic potentials, respectively.
[c]$\Delta E_p = (E_{pa} - E_{pc})$.
[d]E_{pa} refers to the anodic peak potential for the irreversible oxidation waves.
[e]E_{HOMO} levels were calculated from electrochemical potentials, i.e., $E_{HOMO} = -e(E_{pa}+(4.8-F_c^+/F_c))$ or $E_{HOMO} = -e(E_{1/2}+(4.8-F_c^+/F_c))$. ($F_c^+/F_c$ = 0.46 V in CH_2Cl_2).
[f]LUMO = HOMO + E_g (where E_g = optical band gap, which is defined as the onset of absorption).

In order to investigate the electronic structures and the nature of the absorption and emission origins of the Ir(III) complexes, DFT and TD-DFT calculations have been performed on **Ir-1-3** at the B3LYP level of theory. The simulated UV-vis absorption spectra of **Ir-1-3** are shown in Figures S32–S34, in which the computed singlet-triplet transitions with arbitrary oscillator strengths are shown in the inset. The first fifteen singlet-singlet transitions computed by the TD-DFT/PCM (CH_2Cl_2) method are summarized in Table S4, and the frontier molecular orbitals involved in the major transitions are shown in Figures S35–S37. The first four singlet-triplet transitions of **Ir-1-3** were computed at 350–400 nm, which is consistent with the weak absorption band observed in the range of 350–400 nm in the experiment, and they can be assigned as ^{3}MLCT transition mixing with $^3\pi\rightarrow\pi^*$ transition. The intense absorption band computed at ca. 310 nm mainly originates from the HOMO–2→LUMO transition, where the HOMO–2 is the d_π orbital on the metal center mixing with the π orbital localized on the bidentate C^C ligand, and the LUMO is the π^* orbital localized on the pyridylimidazole moiety of the C^C ligand. Therefore, the absorption band at ca. 310 nm can be assigned as ^{1}MLCT[$d\pi$(Ir)→π^*(C^C)] transition, mixing with ^{1}IL transition of the C^C ligand with CT from the phenyl ring to the pyridylimidazole moiety.

Orbital energy calculation

The energies of the frontier molecular orbitals of **Ir-1-3** at their ground states are shown in the orbital energy level diagram in Figure 3. Since the LUMOs of **Ir-1-3** are localized on the pyridylimidazole moiety of the C^C ligand, which is less affected by the substituent on the phenyl ring, their energies do not show much variation and have values of ca. −1.20 eV. The HOMO energy of **Ir-2** (−5.30 eV) is slightly more negative than those of **Ir-1** (−5.24 eV) and **Ir-3** (−5.21 eV) because part of the HOMO is on the phenyl ring of the C^C ligand, and so the electron-withdrawing fluoro group would stabilize the HOMO of **Ir-2**. Both the trends of the HOMO and LUMO energies are in good agreement with that observed in the electrochemical study.

The geometry of the lowest-lying triplet excited states (T_1) of **Ir-1-3** have been optimized with the unrestricted UB3LYP/PCM (CH_2Cl_2) method to further investigate the nature of the emissive state. The plots of spin density of the T_1 states of **Ir-1-3** are shown in Figure S38. For all three complexes, the spin density is predominantly localized on the C^C ligand and the metal center, supporting the ^{3}MLCT and ^{3}IL with CT character of the T_1 state. The emission wavelengths of **Ir-1-3**, approximated by the energy difference between the S_0 and the T_1 states, are summarized in Table S5.

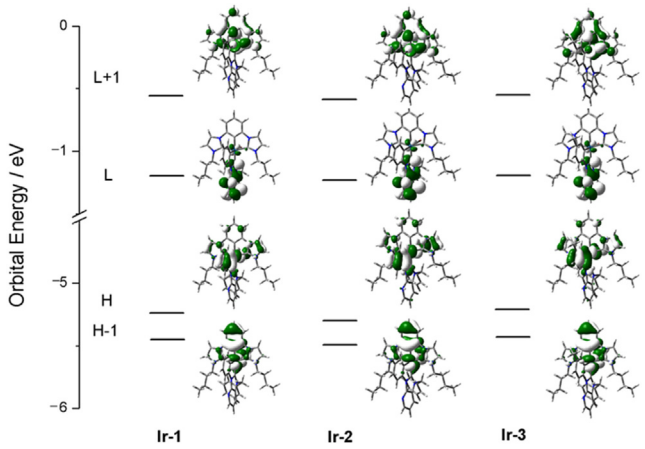

Figure 3. Calculated frontier orbital distributions

Orbital energy level diagram of the frontier molecular orbitals (H = HOMO and L = LUMO) of **Ir1-3** at their optimized ground-state geometries.

The emission wavelengths of the three complexes are ca. 400 nm and do not show significant variation. This agrees with the results obtained in the photophysical study that the emission wavelengths were measured to be ca. 430 nm.

WOLED measurements

The excellent solid-state luminescence properties of **Ir-2** make it a promising candidate for phosphor-converted WLEDs. A series of WLEDs based on 365-nm LED chips were fabricated. The iridium(III) complex was used as phosphors and blended in silicone at a concentration of 5 wt %. The performance and detailed information of those WLEDs are shown in Figure 4 and Table S12. Figure 4A exhibits spectra and typical working state photographs of these WLEDs, and the correlated color temperature and color rendering index (Ra) of obtained WLEDs could be effectively tuned down from 6,428 to 9,832 K and 81.2 to 86.2, respectively, performing better than commercial phosphors. It can be seen in Figures 4B and 4C that the PL spectrum and chromaticity coordinates of these WLEDs in the CIE chromaticity diagram change with the load currents. When the driving current is increased, the luminous efficiency of LED chip will be stronger, which allows more complexes to be excited. The low-energy band of spectra of WLEDs gradually increases, resulting in the CIE coordinates moving to the upper right. The results indicate that **Ir-2** can realize a series of WLEDs with different color temperatures, promising phosphor for WLEDs for white light illumination.

To obtain the electroluminescent properties of the Ir(III) complexes, OLEDs with a device structure of (ITO/(HAT-CN) (10 nm)/TAPC (40 nm)/TCTA (10 nm)/x wt % dopant in DPEPO (10 nm)/TmPyPB (40 nm)/Liq (2.5 nm)/Al (100 nm)) have been fabricated. HAT-CN served as a hole-injection layer, TAPC (1,1-bis{4-[N,N-di(*p*-tolyl)amino] phenyl}cyclohexane) served as a hole-transporting layer, TCTA (4,4,4-Tris(carbazol-9-yl)-triphenylamine) served as an electron-blocking layer to prevent the formation of an exciplex between TAPC and the EMLs, TmPyPB (3,3′-[5′-[3-(3-pyridinyl) phenyl][1,1′:3′,1″-terphenyl]-3,′′-diyl]bispyridine) served as an electron-transporting layer, and Liq (8-hydroxyquinoline lithium) served as an electron-injection layer, with ITO (indium-tin oxide) anode and Al cathode. The excitation and emission spectra of the thin films with **Ir-2** doped in host DPEPO at different concentrations are shown in Figure S39. It can be seen from the excitation spectrum that with the increase of doping concentration, the peak intensity of 319 nm increases, which can be

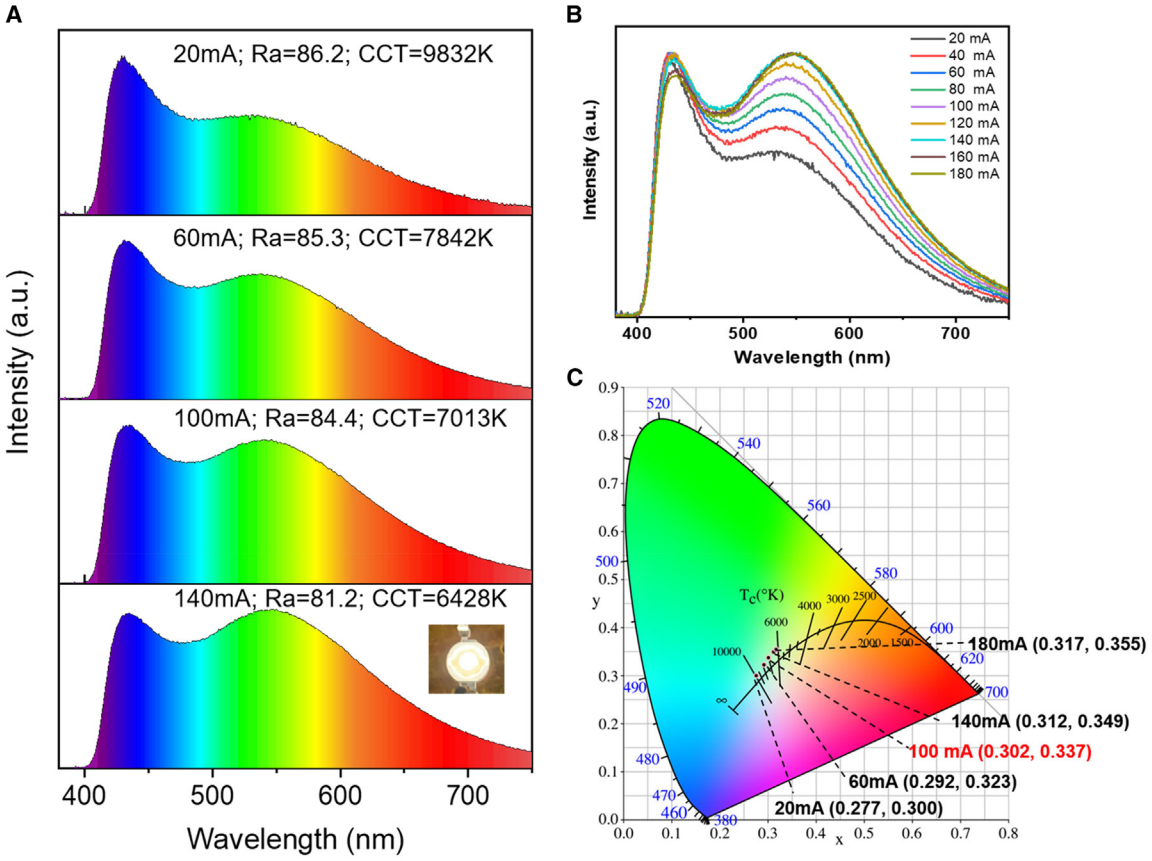

Figure 4. Performance of WLEDs

(A) The photoluminescence spectra of the blue GaN-based WLEDs using **Ir-2** as phosphors blended in silicone at different currents; inset: image of the WLEDs in working state.

(B) The photoluminescence spectra of the WLEDs at different driving currents.

(C) CIE chromaticity coordinates of the WLEDs with the phosphor blended at different currents.

assigned to the PL band in the low-energy region. In order to obtain obvious white light emission in the device, **Ir-2** was doped in DPEPO at different concentrations of x wt % (x = 20, 30, 40, 50, 60) in the emitting layer. The device structure with its energy level diagram is shown in Figure 5A. The electroluminescent properties results are summarized in Table 3.

The OLED with **Ir-2** as an active layer showed a lower turn-on voltage of 3.0 V, a maximum EQE of 6.2%, and a maximum luminance (L_{max}) of 335 cd m^{-2} at 30 wt %. Simultaneously, the white light with a CIE coordinate of (0.31, 0.33) was achieved successfully, which was very close to the standard white light, as shown in the inset of Figure 5B. Furthermore, complexes **Ir-1** and **Ir-3** have also been fabricated with the device structure at 30 wt %. Figure 5 shows the electroluminescence properties based on different guests **Ir-1-3**. The EL spectra of these devices were redshifted by ca. 60 nm compared to the PL spectra in solid. Meanwhile, the intensity of the low-energy peak of **Ir-2** is larger than that of **Ir-1** and **Ir-3**, which is consistent with the previous experimental data. Among them, the device based on **Ir-2** exhibited better performance due to its higher PLQY than the others.

Here, we design and synthesize three organometallic iridium(III) complexes, which show bright solid-state white-light emission at room temperature. The white light

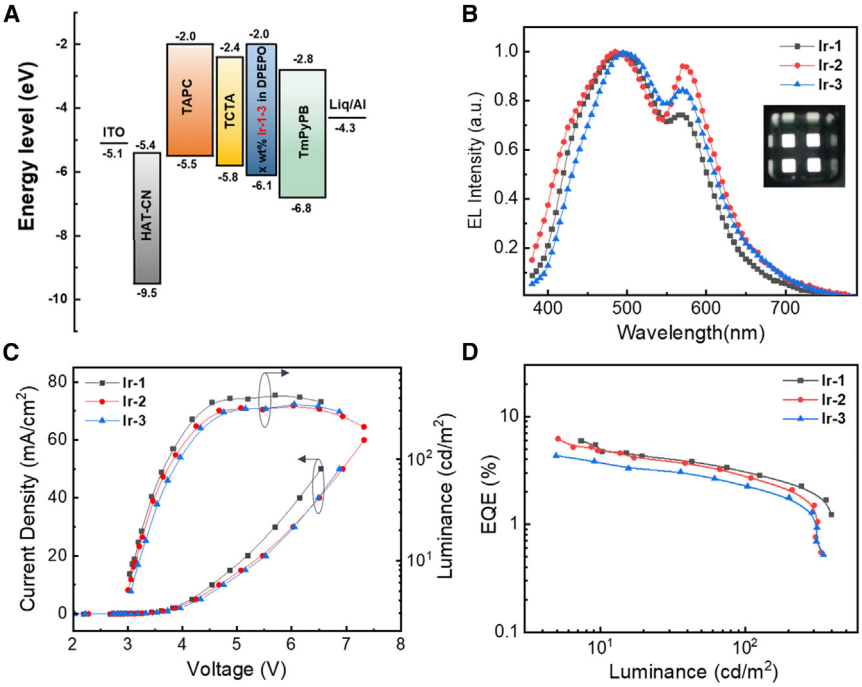

Figure 5. Electroluminescence performances of Ir-1-3 in doped OLEDs

(A) Device structure and energy level of the electroluminescent device.

(B) EL spectra. Inset: the photograph of the electroluminescent device in working state.

(C) Current density-voltage-luminance (J-V-L) characteristics.

(D) EQE vs. luminance.

comes from dual-phosphorescent emission at the high-energy blue region and the low-energy yellow region. The emission shows a mixed character of ^{3}MLCT, ^{3}LLCT, and ^{3}ILCT. The molecular orientation and stacking affect the emission color and PLQY, especially the low-energy peak. The DFT and TD-DFT calculations suggest the π-π interaction between tridentate ligands of two adjacent molecules excites the metal to ligand charge transfer (^{3}MLLCT), which enhances phosphorescence emission in the solid state to a quantum photoluminescence yield of 14%. **Ir-2** exhibits notable single-component photoluminescence and electroluminescence properties. The WLEDs

Table 3. Device performance data of Ir-1-3 doped in DPEPO

Dopant	Conc. [x wt %]	V_{on}[a] [V]	L_{max}[b] [cd m^{-2}]	λ_{max}[c] [nm]	CIE [x,y][d]	η_{Ext}[e] [%]	η_L[f] [cd A^{-1}]	η_P[g] [lm W^{-1}]
Ir-2	20	3.1	346	485, (572)	(0.29, 0.30)	5.8	11.7	11.8
–	30	3.0	335	485, (572)	(0.31, 0.33)	6.2	12.7	13.3
–	40	3.0	281	485, (572)	(0.28, 0.30)	5.4	10.8	11.3
–	50	3.0	262	495, (573)	(0.32, 0.34)	4.3	9.3	9.7
–	60	3.0	219	492, (573)	(0.29, 0.31)	3.8	7.7	8.0
Ir-1	30	3.0	427	497, (571)	(0.26, 0.30)	5.9	12.2	12.7
Ir-3	30	3.1	314	498, (571)	(0.26, 0.31)	4.3	10.1	10.1

[a]At 1 cd/m^2.

[b]Maximum luminance (L_{max}).

[c]Peak maximum (λ_{max}).

[d]CIE coordinates at 100 cd m^{-2}.

[e]Maximum external quantum efficiency (η_{Ext}).

[f]Maximum current efficiency (η_L).

[g]Maximum power efficiency (η_P).

based on **Ir-2** show a best CRI of 86.2, higher than the commercial LED of 78. The OLED with **Ir-2** as an active layer exhibits a low turn-on voltage of 3.0 V, a maximum *EQE* of 6.2%, and a maximum luminance (L_{max}) of 335 cd m^{-2} with CIE coordinate of (0.31, 0.33). Our results provide a strategy to achieve single-component white OLEDs based on iridium(III) complexes.

EXPERIMENTAL PROCEDURES

Resource availability

Lead contact

Further information and requests for resources should be directed to and will be fulfilled by the lead contact, Guodan Wei (weiguodan@sz.tsinghua.edu.cn).

Materials availability

The target molecules can be produced following the procedures in the section of materials synthesis in the supplemental experimental procedures. Any additional information or requests for materials will be handled by the lead contact upon reasonable request.

Data and code availability

The accession number for the single-crystal structure of **Ir-2** reported in this paper is CCDC: 2241509. The datasets generated during this study are presented within the article and supplemental information or can be provided by the authors upon reasonable request.

SUPPLEMENTAL INFORMATION

Supplemental information can be found online at https://doi.org/10.1016/j.xcrp.2023.101684.

ACKNOWLEDGMENTS

The authors thank the support of the National Natural Science Foundation of China (grant nos. 52027817, 22275114); Shenzhen Science and Technology Innovation Committee (grant nos. GJHZ20210705143204013, WDZC20220817160017003); Cross-Disciplinary Research Fund of Tsinghua Shenzhen International Graduate School (SIGS), Tsinghua University (JC2022003); Scientific Research Startup Fund of SIGS, Tsinghua University (grant no. QD2021027c); and Shenzhen Science and Technology Innovation Committee (JCYJ20200109144614514).

AUTHOR CONTRIBUTIONS

M.Z. synthesized the molecules. W.L. performed photophysical property measurements and fabricated photoluminescent devices. M.Z. prepared and characterized OLED devices. M.N. and C.W. performed theoretical computations. Z.M., W.L., and S.-W.Z. wrote and revised the manuscript. M.-C.T., C.Y., and G.W. supervised the project. All authors contributed to commenting on and editing the manuscript.

DECLARATION OF INTERESTS

The authors declare no conflict of interest.

Received: July 14, 2023
Revised: August 31, 2023
Accepted: October 25, 2023
Published: November 17, 2023

REFERENCES

1. D'Andrade, B.W., and Forrest, S.R. (2004). White organic light-emitting devices for solid-state lighting. Adv. Mater. *16*, 1585–1595. https://doi.org/10.1002/adma.200400684.

2. Li, W., Wang, Z., Zhang, M., He, M., Zhang, S.W., Yang, C., Wu, Y., Li, J., Tang, M.C., Fu, H., and Wei, G. (2022). Efficient yellow phosphorescent [3+2+1] Ir (III) complex for warm white lighting and visible light communication. Mater. Today Energy *23*, 100892. https://doi.org/10.1016/j.mtener.2021.100892.

3. Stanitska, M., Mahmoudi, M., Pokhodylo, N., Lytvyn, R., Volyniuk, D., Tomkeviciene, A., Keruckiene, R., Obushak, M., and Grazulevicius, J.V. (2022). Exciplex-forming systems of physically mixed and covalently bonded benzoyl-1H-1,2,3-triazole and carbazole moieties for solution-processed white OLEDs. J. Org. Chem. *87*, 4040–4050. https://doi.org/10.1021/acs.joc.1c02784.

4. Chen, Z., Ho, C.L., Wang, L., and Wong, W.Y. (2020). Single-molecular white-light emitters and their potential WOLED applications. Adv. Mater. *32*, 1903269. https://doi.org/10.1002/adma.201903269.

5. Wang, Q., Ding, J., Ma, D., Cheng, Y., Wang, L., Jing, X., and Wang, F. (2009). Harvesting excitons via two parallel channels for efficient white organic LEDs with nearly 100% internal quantum efficiency: fabrication and emission-mechanism analysis. Adv. Funct. Mater. *19*, 84–95. https://doi.org/10.1002/adfm.200800918.

6. Mahmoudi, M., Keruckas, J., Leitonas, K., Kutsiy, S., Volyniuk, D., and Gražulevičius, J.V. (2021). Exciplex-forming systems with extremely high RISC rates exceeding 10^7 s^{-1} for oxygen probing and white hybrid OLEDs. J. Mater. Res. Technol. *10*, 711–721. https://doi.org/10.1016/j.jmrt.2020.12.058.

7. Sun, Y., Giebink, N.C., Kanno, H., Ma, B., Thompson, M.E., and Forrest, S.R. (2006). Management of singlet and triplet excitons for efficient white organic light-emitting devices. Nature *440*, 908–912. https://doi.org/10.1038/nature04645.

8. Sun, Y., and Forrest, S.R. (2008). Enhanced light out-coupling of organic light-emitting devices using embedded low-index grids. Nat. Photonics *2*, 483–487. https://doi.org/10.1038/nphoton.2008.132.

9. Chatsirisupachai, J., Nalaoh, P., Kaiyasuan, C., Chasing, P., Sudyoadsuk, T., and Promarak, V. (2021). Unique dual fluorescence emission in the solid state from a small molecule based on phenanthrocarbazole with an AIE luminogen as a single-molecule white-light emissive material. Mater. Chem. Front. *5*, 2361–2372. https://doi.org/10.1039/D0QM00951B.

10. Li, C., Liang, J., Liang, B., Li, Z., Cheng, Z., Yang, G., and Wang, Y. (2019). An organic emitter displaying dual emissions and efficient delayed fluorescence white OLEDs. Adv. Opt. Mater. *7*, 1801667. https://doi.org/10.1002/adom.201801667.

11. Khan, F., Volyniuk, L., Ghasemi, M., Volyniuk, D., Grazulevicius, J.V., and Misra, R. (2022). Efficient monomolecular white emission of phenothiazine boronic ester derivatives with room temperature phosphorescence. J. Mater. Chem. C *10*, 10347–10355. https://doi.org/10.1039/D2TC01612E.

12. Pati, A.K., Mohapatra, M., Ghosh, P., Gharpure, S.J., and Mishra, A.K. (2013). Deciphering the photophysical role of conjugated diyne in butadiynyl fluorophores: synthesis, photophysical and theoretical study. J. Phys. Chem. A *117*, 6548–6560. https://doi.org/10.1021/jp404809g.

13. Lee, J., Kim, B., Kwon, J.E., Kim, J., Yokoyama, D., Suzuki, K., Nishimura, H., Wakamiya, A., Park, S.Y., and Park, J. (2014). Excimer formation in organic emitter films associated with a molecular orientation promoted by steric hindrance. Chem. Commun. *50*, 14145–14148. https://doi.org/10.1039/C4CC05348F.

14. Coppo, P., Duati, M., Kozhevnikov, V.N., Hofstraat, J.W., and De Cola, L. (2005). White-light emission from an assembly comprising luminescent iridium and europium complexes. Angew. Chem. *117*, 1840–1844. https://doi.org/10.1002/ange.200461953.

15. Kwon, J.E., and Park, S.Y. (2011). Advanced organic optoelectronic materials: harnessing excited-state intramolecular proton transfer (ESIPT) process. Adv. Mater. *23*, 3615–3642. https://doi.org/10.1002/adma.201102046.

16. Zhou, G., Wang, Q., Ho, C.L., Wong, W.Y., Ma, D., and Wang, L. (2009). Duplicating "sunlight" from simple WOLEDs for lighting applications. Chem. Commun. *3574–3576*, 3574–3576. https://doi.org/10.1039/B904382A.

17. Zhou, G., Wang, Q., Wang, X., Ho, C.L., Wong, W.Y., Ma, D., Wang, L., and Lin, Z. (2010). Metallophosphors of platinum with distinct main-group elements: a versatile approach towards color tuning and white-light emission with superior efficiency/color quality/brightness trade-offs. J. Mater. Chem. *20*, 7472–7484. https://doi.org/10.1039/C0JM01159B.

18. Muñoz-Rodríguez, R., Buñuel, E., Fuentes, N., Williams, J.A.G., and Cárdenas, D.J. (2015). A heterotrimetallic Ir(III), Au(III) and Pt(II) complex incorporating cyclometallating bi- and tridentate ligands: simultaneous emission from different luminescent metal centres leads to broad-band light emission. Dalton Trans. *44*, 8394–8405. https://doi.org/10.1039/C4DT02761B.

19. Zhao, X., Alam, P., Zhang, J., Lin, S., Peng, Q., Zhang, J., Liang, G., Chen, S., Zhang, J., Sung, H.H.Y., et al. (2022). Metallophilicity-induced clusterization: single-component white-light clusteroluminescence with stimuli responses. CCS Chem. *4*, 2570–2580. https://doi.org/10.31635/ccschem.021.202101392.

20. Bin Mohd Yusoff, A.R., Huckaba, A.J., and Nazeeruddin, M.K. (2017). Phosphorescent neutral iridium (III) complexes for organic light-emitting diodes. Top. Curr. Chem. *375*, 39. https://doi.org/10.1007/s41061-017-0126-7.

21. Wang, T., Shi, M., Fang, D., He, J., Zhang, M., Zhang, S., Wei, G., and Meng, H. (2021). Novel spiro[fluorene-9,9′-xanthene]-based hole transport layers for red and green PHOLED devices with high efficiency and low efficiency roll-off. J. Mater. Chem. C *9*, 3247–3256. https://doi.org/10.1039/D0TC04676K.

22. Yeh, Y.S., Cheng, Y.M., Chou, P.T., Lee, G.H., Yang, C.H., Chi, Y., Shu, C.F., and Wang, C.H. (2006). A new family of homoleptic Ir(III) complexes: tris-pyridyl azolate derivatives with dual phosphorescence. ChemPhysChem *7*, 2294–2297. https://doi.org/10.1002/cphc.200600461.

23. Kumar, S., Hisamatsu, Y., Tamaki, Y., Ishitani, O., and Aoki, S. (2016). Design and synthesis of heteroleptic cyclometalated iridium(III) complexes containing quinoline-type ligands that exhibit dual phosphorescence. Inorg. Chem. *55*, 3829–3843. https://doi.org/10.1021/acs.inorgchem.5b02872.

24. Zhang, K.Y., Gao, P., Sun, G., Zhang, T., Li, X., Liu, S., Zhao, Q., Lo, K.K.W., and Huang, W. (2018). Dual-phosphorescent iridium(III) complexes extending oxygen sensing from hypoxia to hyperoxia. J. Am. Chem. Soc. *140*, 7827–7834. https://doi.org/10.1021/jacs.8b02492.

25. King, K.A., and Watts, R.J. (1987). Dual emission from an ortho-metalated iridium(III) complex. J. Am. Chem. Soc. *109*, 1589–1590. https://doi.org/10.1021/ja00239a060.

26. Pomarico, E., Silatani, M., Messina, F., Braem, O., Cannizzo, A., Barranoff, E., Klein, J.H., Lambert, C., and Chergui, M. (2016). Dual luminescence, interligand decay, and nonradiative electronic relaxation of cyclometalated iridium complexes in solution. J. Phys. Chem. C *120*, 16459–16469. https://doi.org/10.1021/acs.jpcc.6b04896.

27. Benjamin, H., Zheng, Y., Kozhevnikov, V.N., Siddle, J.S., O'Driscoll, L.J., Fox, M.A., Batsanov, A.S., Griffiths, G.C., Dias, F.B., Monkman, A.P., and Bryce, M.R. (2020). Unusual dual-emissive heteroleptic iridium complexes incorporating TADF cyclometalating ligands. Dalton Trans. *49*, 2190–2208. https://doi.org/10.1039/C9DT04672K.

28. Ladouceur, S., Donato, L., Romain, M., Mudraboyina, B.P., Johansen, M.B., Wisner, J.A., and Zysman-Colman, E. (2013). A rare case of dual emission in a neutral heteroleptic iridium(III) complex. Dalton Trans. *42*, 8838–8847. https://doi.org/10.1039/C3DT33115F.

29. Lo, K.K.W., Zhang, K.Y., Leung, S.K., and Tang, M.C. (2008). Exploitation of the dual-emissive properties of cyclometalated iridium(III)-polypyridine complexes in the development of luminescent biological probes. Angew. Chem. Int. Ed. *47*, 2213–2216. https://doi.org/10.1002/anie.200705155.

30. Liu, Z., Zhang, S.W., Zhang, M., Wu, C., Li, W., Wu, Y., Yang, C., Kang, F., Meng, H., and Wei, G. (2021). Highly efficient phosphorescent blue-emitting [3+2+1] coordinated iridium (III) complex for OLED application. Front. Chem. *9*, 758357. https://doi.org/10.3389/fchem.2021.758357.

31. Zhang, M., Ng, M., Wu, C., Tong, K.N., Li, W., Wu, Y., Yang, C., Wang, M., Tang, M.C., and Wei, G. (2022). Saturated-blue-emitting [3+2+1] coordinated iridium(iii) complexes for vacuum-deposited organic light-emitting

devices. J. Mater. Chem. C *10*, 14616–14625. https://doi.org/10.1039/D2TC02829H.

32. Wu, C., Tong, K.N., Zhang, M., Ng, M., Zhang, S.W., Cai, W., Jung, S., Wu, Y., Yang, C., Tang, M.C., and Wei, G. (2022). Low efficiency roll-off blue phosphorescent OLEDs at high brightness based on [3+2+1] coordinated iridium (III) complexes. Adv. Opt. Mater. *10*, 2200356. https://doi.org/10.1002/adom.202200356.

33. Vargas, V.C., Rubio, R.J., Hollis, T.K., Salcido, M.E., and Salcido, M.E. (2003). Efficient route to1,3-di-N-imidazolylbenzene. A comparison of monodentate vs bidentate carbenes in Pd-catalyzed cross coupling. Org. Lett. *5*, 4847–4849. https://doi.org/10.1021/ol035906z.

34. Charra, V., de Frémont, P., Breuil, P.A.R., Olivier-Bourbigou, H., and Braunstein, P. (2015). Silver(I) and copper(I) complexes with bis-NHC ligands: Dinuclear complexes, cubanes and coordination polymers. J. Organomet. Chem. *795*, 25–33. https://doi.org/10.1016/j.jorganchem.2015.01.025.

35. Zhang, M., Zhang, S.W., Wu, C., Li, W., Wu, Y., Yang, C., Meng, Z., Xu, W., Tang, M.C., Xie, R., et al. (2022). Fine emission tuning from near-ultraviolet to saturated blue with rationally designed carbene-based [3 + 2 + 1] iridium(III) complexes. ACS Appl. Mater. Interfaces *14*, 1546–1556. https://doi.org/10.1021/acsami.1c19127.

36. Kuei, C.Y., Tsai, W.L., Tong, B., Jiao, M., Lee, W.K., Chi, Y., Wu, C.C., Liu, S.H., Lee, G.H., and Chou, P.T. (2016). Bis-tridentate Ir(III) complexes with nearly unitary RGB phosphorescence and organic Light-Emitting diodes with external quantum efficiency exceeding 31. Adv. Mater. *28*, 2795–2800. https://doi.org/10.1002/adma.201505790.

37. Wu, Y., Yang, C., Liu, J., Zhang, M., Liu, W., Li, W., Wu, C., Cheng, G., Yang, Q., Wei, G., and Che, C.M. (2021). Phosphorescent [3+2+1] coordinated Ir(iii) cyano complexes for achieving efficient phosphors and their application in OLED devices. Chem. Sci. *12*, 10165–10178. https://doi.org/10.1039/D1SC01426A.